Theoretical and Applied Fracture Mechanics 110 (2020) 102799

Contents lists available at ScienceDirect

Theoretical and Applied Fracture Mechanics

journal homepage: www.elsevier.com/locate/tafmec

Experimental study of the relationship between fracture initiation toughness and brittle crack arrest toughness predicted from small-scale testing

Jessica Taylor [a,b], Ali Mehmanparast [a,*], Rob Kulka [c], Philippa Moore [c], Li Xu [d], Gholam Hossein Farrahi [a,e]

[a] Offshore Renewable Energy Engineering Centre, Cranfield University, Cranfield, Bedfordshire MK43 0AL, UK
[b] NSIRC, TWI Ltd, Granta Park, Great Abington, Cambridge CB21 6AL, UK
[c] TWI, Granta Park, Cambridge CB21 6AL, UK
[d] Lloyd's Register, Global Technology Centre, Southampton SO16 7QF, UK
[e] School of Mechanical Engineering, Sharif University of Technology, Tehran, Iran

ARTICLE INFO

Keywords:
Brittle crack arrest
Structural steel
Small-scale testing
Fracture toughness
Crack arrest toughness

ABSTRACT

It is vital to prevent brittle cracks in large structures. This is particularly important for a number of industry sectors including offshore wind, Oil & Gas, and shipbuilding where structural failure risks loss of human life and loss of expensive assets. Some modern steels exhibit high Charpy energy – i.e. high initiation fracture toughness, but poor resistance to crack propagation – i.e. low crack arrest toughness. The correlation between initiation and arrest toughness measured through small-scale testing is investigated in five different steels, which include S355 structural steel (with two different thicknesses), X65 pipeline steel, two high strength reactor pressure vessel steels and EH47 shipbuilding steel. Small scale mechanical tests were carried out to characterise the materials' properties and were compared to the materials' microstructures. A wide range of tests were carried out, including instrumented Charpy, drop weight Pellini, fracture toughness, tensile testing, and optical microscopy. Nil ductility transition temperature (NDTT) is used to characterise a material's arrest properties. Initiation fracture toughness correlated with higher upper shelf Charpy energy and smaller average grain sizes, as expected, however none of these correlated well with the arrest toughness measured through NDTT. The NDTT correlated most strongly with the T_{27J} temperature which indicates the start of lower shelf of the Charpy curve. This correlation held for all materials including those where the NDTT lies on the upper shelf of the Charpy curve. While initiation fracture toughness can be predicted through high Charpy toughness and operation temperatures on the upper shelf, crack arrest behaviour should be predicted from characteristics of the ductile to brittle transition temperature, for example by using the T_{4kN} from instrumented Charpy tests or T_{27J}.

1. Introduction

Crack initiation and propagation is often experienced by engineering components and structures subjected to operational loading conditions. An important issue that needs to be understood for design and life assessment of such structures is the ability of a material to arrest a fast-running brittle crack, particularly for structures where fracture may initiate in areas of high local stress or low toughness, for example in the welds [1]. This is particularly important for a number of industry sectors including offshore wind, Oil & Gas, and shipbuilding where structural failure risks loss of human life and loss of expensive assets. The load cannot be transferred through a crack, so once it grows too large the whole structure will fail.

Structures in offshore environments are exposed to very harsh loading conditions, with both wind and wave loading in addition to the operating loads i.e. its own mass and moving components [2,3]. In such structures a crack may initiate around a weld region, which is the part of a structure most susceptible to cracking due to material mismatch, heat input which changes material properties, locked-in residual stresses and increased chance of impurity inclusions during the welding process [4]. Smaller components can be heat-treated after welding, to reduce the damaging effects of welding residual stresses and reset the materials microstructure and larger structures can receive local heat treatment

* Corresponding author.
E-mail address: a.mehmanparast@cranfield.ac.uk (A. Mehmanparast).

https://doi.org/10.1016/j.tafmec.2020.102799
Received 3 July 2020; Received in revised form 8 October 2020; Accepted 9 October 2020
Available online 13 October 2020

Nomenclature

a	Crack length
a_0	Initial crack length
B	Thickness
E	Elastic Young's modulus
K_a	Crack arrest toughness
K_{ca}	Crack arrest toughness: lower bound approximation measured following ASTM E1221
K_{Ia}	Crack arrest toughness: critical stress intensity factor for crack arrest under mode I fracture mechanics loading condition
K_{IC}	Initiation fracture toughness: critical stress intensity factor for crack initiation under mode I fracture mechanics loading condition
K_{JC}	an elastic-plastic equivalent stress intensity factor derived from the J-integral at the point of onset of cleavage fracture.
σ_y	Yield strength
T	Temperature
T_0	Reference temperature at which a material's initiation fracture toughness is 100 MPa$\sqrt{m}$
T_{27J}	Reference temperature at which a material's Charpy impact energy is 27 J
T_{4kN}	Reference temperature at which a material's arrest force during instrumented Charpy test is 4kN
T_{KIa}	Reference temperature at which a material's arrest toughness is 100 MPa$\sqrt{m}$
ASME	American Society of Mechanical Engineers
CAT	Crack Arrest Temperature
CTOD	Crack Tip Opening Displacement
CVN	Charpy V Notch
EBSD	Electron Backscatter Diffraction
NDTT	Nil Ductility Transition Temperature
RoA	Reduction of Area
RPV	Reactor Pressure Vessel
SEN(B)	Single Edge Notched Bend fracture toughness test
STRA	Short Transverse Reduction of Area
UTS	Ultimate Tensile Strength

[4]. However, this is simply not commercially viable for very large components such as ships, wind turbine support structures, or long welded pipelines.

An alternative approach to initiation prevention is the crack arrest approach. Using this concept, it can be considered that fracture may occur in a local region of high stress, embrittlement or under accidental damage. However the material's properties are carefully controlled so it has a sufficient toughness to inhibit fracture propagation outside this region [5]. When the crack arrests before growing too long, catastrophic failure can be prevented. This is vital for a structure with welds, which can be a hotspot for defects or embrittled zones which promote fracture initiation. Moreover, the crack arrest approach can be more reliable than the initiation approach at preventing catastrophic fracture as it accounts for accidental damage and is effective even once a crack is growing [6].

If brittle fracture occurs in a high toughness steel, the initial driving force can be incredibly high, which means the crack will not arrest but propagates until the whole structure fails. This means that some modern steels with very high fracture initiation toughness can be at risk of poor crack arrest behaviour if an accident occurs. This may be a concern for some modern steels which have a very good Charpy toughness, but a poor resistance to fracture propagation [7,8]. In structures made of such materials, accidental damage could result in total structural failure due to the lack of conservatism when brittle crack arrest is not considered. In fact, it has recently been shown that although a smaller average grain size improves fracture initiation toughness, it will worsen the brittle crack arrest toughness [9]. In addition, a material's crack arrest properties are heavily temperature dependent for materials which exhibit ductile to brittle transition i.e. ferritic steels. It may be considered that ductile behaviour will occur if a material is operating ats a temperature on its upper shelf, but this is not always assured [7]. An example could be impact or dynamic loading where the material experiences a shift upwards of the ductile to brittle transition temperature compared to quasi-static loading behavior [10]; i.e. steels operating at temperatures on their upper shelf can experience brittle crack initiation under dynamic load events such as crash, impact or earthquakes.

In recent years, a number of successful numerical models have been developed to simulate and predict crack arrest in steels. Through adaptation of models used to describe fracture initiation, the mechanism behind crack propagation and arrest is understood to be governed by the local stress criterion [11–20]. That is, crack propagation is determined by the stress state a short distance ahead of the crack tip. This is commonly assessed using the RKR criterion which was originally developed to predict fracture initiation toughness [21]. This can be further explained through grain-scale micromechanical models [22–25]. Alongside the recent theoretical advances explaining the mechanism behind crack arrest, there is interest in determining which small-scale test methods are effective at predicting crack arrest behaviour and how a material's different mechanical properties are related to one another.

The purpose of this study is to develop a better understanding of the crack arrest behaviour in a range of modern steels by performing mechanical testing and metallurgical analysis of the materials' microstructures, which have been suggested to influence crack arrest properties [9,26–29]. The results from this study correlate the mechanical properties with the microstructure of five different modern structural steels to evaluate the relevant parameters necessary for fracture prevention.

2. Empirical test methods for evaluating crack arrest

Crack arrest properties are typically measured by one of the following two parameters; 1-crack arrest toughness, K_a, or 2- crack arrest temperature (CAT). The crack arrest toughness, K_a, can be defined as the critical stress intensity factor for crack arrest under the mode I fracture mechanics loading condition above which a fast-running crack is arrested, K_{ca}. Alternatively, a lower bound approximation of crack arrest toughness, K_{Ia}, can be used, although this may give a conservative estimate [30–32]. The CAT is the lowest temperature that a fast-running brittle crack will arrest in a certain material under specified conditions. The CAT can be determined by initiating a brittle crack in a material at a range of temperatures and finding the lowest temperature where a brittle running crack arrests [5]. In such experiments, fracture is typically initiated by impacting a region with a notched brittle weld bead. K_{Ia} and K_{ca} can be determined through standardised methods such as those described in ASTM E1221 and JWES 2815 [33–35].

Although many empirical equations are available in the literature to predict the structural behaviour in terms of crack arrestibility from small-scale test results, very few standards recommend the use of them. The only mention is in the R6 defect tolerance assessment procedure, which recommends the use of drop weight Pellini testing for applications in the UK nuclear industry [36]. This is because as the dimensions and particularly the thickness of the plates employed in many industrial applications increase, the empirical equations are no longer valid, and may not fully describe the crack arrest behaviour of actual structures.

Table 1
Summary of small-scale testing carried out and specimen geometries.

Test type	Number of specimens for each material	Extraction location	Orientation (of notch or gauge region)	Thickness, B (mm)	Width, W (mm)	Length, L (mm)
Tensile Roundbar (BS EN ISO 6892-1)	3	Mid-thickness	Along rolling direction if known	8 (gauge diameter)	n/a	48 (gauge length)
Tensile STRA (BS EN 10164)	3	Through-thickness	Through-thickness	10 (gauge diameter), reduced to 6 (gauge diameter for materials of 30 mm thickness or less)	n/a	Full plate thickness
Instrumented Charpy V Notch (BS EN ISO 148-1)	20	Mid-thickness	Transverse to rolling direction	10	10	55
Pellini - P2 size (ASTM E208)	8+ (if more needed to determine NDTT)	Quarter wall	Through-thickness	19	50	130
SEN(B) Fracture Toughness (BS 7448-1)	3	Mid-thickness	Transverse to rolling direction	20	20	120

Although crack arrest toughness is thought of as a material property, it is strongly dependent on the plate thickness, test temperature, applied stress [37–40]. Furthermore, brittle crack arrest toughness shows a dependence on specimen width as well as manufacturing processes [41–44]. This makes it complex to predict the crack arrest properties of large structures from subsize specimens, thus introduces a need for a sufficiently conservative approach.

2.1. Small-scale testing correlations for steels

The ability of a material to resist growth of a propagating brittle crack is analogous to its crack arrest properties. This is measured using the CAT, the minimum temperature where the material arrests a brittle running fracture. Since crack arrest toughness depends on temperature, the ductile to brittle transition of the material must be understood. Reference temperatures taken from the transitional behaviour include the Charpy impact energy (e.g. temperature at onset of lower shelf) and nil-ductility transition temperature (NDTT) which can be determined through small-scale testing. Empirical relationships are available in the literature to predict the large scale behaviour from these reference temperatures [45,46]. However, the empirical equations are validated for certain specimen dimensions of a given material at a specified thickness, under a certain loading rate. This means that they cannot necessarily be applied to represent a large structure which would almost certainly not meet the strict validity criteria. Therefore some researchers recommend using the NDTT to quantify a material's crack arrest properties [47].

The following relationships were determined by analysing a large amount of data from Charpy-V-Notch (CVN) and drop weight Pellini impact tests. Many other empirical relations are available in the literature and this section highlights just a small number of those [34,48–55]:

$$Pellini\ NDTT = 120J\ CVN\ temperature + 50\ ^\circ\mathrm{C} \quad (1)$$

$$Pellini\ NDTT = 40J\ CVN\ temperature + 60\ ^\circ\mathrm{C} \quad (2)$$

$$Pellini\ NDTT = 27J\ CVN\ temperature + 60\ ^\circ\mathrm{C} \quad (3)$$

Eqs. (1)–(3) can be used to predict the crack arrest temperature by using Eq. (4). This enables use of CVN results to predict the CAT, although of course the NDTT from Pellini testing can be used [5]:

$$CAT = NDTT + 40\ ^\circ\mathrm{C} \quad (4)$$

From the simple relations given above, a range of tests were carried out to make corrections for a variation in applied stress and thickness [47]. This relationship uses the reference conditions of the CAT for 124 MPa applied stress (σ) on a 25 mm thick (B) plate and adds corrections for other stresses and thicknesses. This leads to the semi-empirical Wiesner equation given below, which is valid up to a thickness of 250 mm [5]:

$$CAT = [NDTT + 10] + \left[\frac{\ln[\sigma]}{0.046} - 105\right] + \left[153(B-5)^{\frac{1}{13}} - 190\right]\ ^\circ\mathrm{C} \quad (5)$$

This in turn has led to the formula commonly used today, in the R6 defect tolerance assessment procedure for the UK nuclear industry [36,56]:

$$CAT = NDTT + 21.7\ln\sigma + 173.2(200B-1)^{\frac{1}{13}} - 285\ ^\circ\mathrm{C} \quad (6)$$

The NDTT is the most common parameter which is used to predict the CAT from small-scale test results because there has been a wide range of research into different materials and their weldments. Additionally, the drop weight method measures the ability of the material to resist a propagating brittle crack and can be explained theoretically using fracture mechanics [34,57]. Because of this, NDTT will be used as a measure of crack arrestibility in this work.

2.2. Reference curves

Reference curves are used extensively in the pressure vessel industry to give a lower bound crack initiation toughness for all the grades of pressure vessel steel at temperatures within the transition region [43]. Originally, the American Society of Mechanical Engineers (ASME) reference curve was used in industry [58], which gives an estimate based on extensive experimental results. The master curve approach is an alternative statistical approximation which may give a higher degree of accuracy [59,60]. These approaches use a reference temperature (for example T_0, the temperature corresponding to a mean initiation fracture toughness of 100 MPa$\sqrt{\mathrm{m}}$) for the material to calculate its toughness at a given temperature [43]. The median fracture toughness, K_{JC} is predicted using the following equation:

$$K_{JC(median)} = 30 + 70e^{0.019(T-T_0)} \quad \text{Ref.[43]} \quad (7)$$

where K_{JC} is in MPa$\sqrt{\mathrm{m}}$ and T, the assessment temperature, has the unit of °C (i.e. degrees Celsius). It is assumed that both the initiation toughness, K_{JC}, and lower bound approximation of crack arrest toughness, K_{Ia}, data are expected to exhibit the same temperature dependence since the temperature dependence of both toughness values is controlled by the atomic arrangement, or crystal structure of the material. Consequently, the temperature dependence is expected to be common to all ferritic steels [58]. Through analysis of a large amount of experimental data, the following relations which are relevant to this work were proposed in the literature [58,61]:

$$K_{IC} = 51.276 + 51.897e^{0.036(T-NDTT)} \quad \text{Ref.[61]} \quad (8)$$

$$K_{Ia} = 49.957 + 16.878e^{0.028738(T-NDTT)} \quad \text{Ref.[61]} \quad (9)$$

where K_{IC} and K_{Ia} are in MPa$\sqrt{\mathrm{m}}$ and T, the assessment temperature, has the unit of °C (i.e. degrees Celsius). An alternative correlation which has been developed in previous studies takes the reference temperature from

Table 2
Summary of the different steels used in this research.

Material Reference	M01	M02	M03	M04	M05	M06
Material	RPV A543	RPV A302	X65	S355G10 + M	S355G10 + M	EH47
Thickness (mm)	28	28	30	90	50	80

instrumented Charpy testing to describe the arrest toughness using the temperature at which the force after fracture measured by an instrumented Charpy test is 4 kN, *T4kN* [62].

$$K_{Ia} = 30 + 70e^{\left(\frac{T - T_{4kN} - 12.3}{52.63}\right)} \quad \text{Ref.}[62] \tag{10}$$

Although K_{Ia} will not be determined in this work, the predictions from these methods will be compared with each other to determine their agreement with one another and likely conservatism using K_{Ia} results from other researchers to give realistic K_{Ia} ranges.

3. Experimental procedure and specimen manufacture

The test program and specimen key information are summarised in Table 1, with further details explained below. The materials used are summarised in Table 2.

Where possible, the specimen orientation and extraction location were kept the same for each material, however this was not always possible. For example, no matter the extraction location, a 19 mm thick Pellini specimen will sample a larger proportion of the 28 mm thick steel plate than the 90 mm thick steel plate. Similarly, it was decided to use only subsize SEN(B) fracture toughness tests rather than full plate thickness (as is recommended in the standard) to be able to limit the size effects which could not be captured through the other test methods and make the results more comparable to each other. The rolling direction was not known for materials M05 and M06. The specimen extraction plan is shown in Appendix A.

Drop weight Pellini testing was carried out using Pellini P2 specimens (with dimensions given in Table 1), following ASTM E208 [34], to measure the NDTT of each material from which CAT can be estimated. Pellini specimens were made up of a small block of material on which a brittle weld bead was laid using a hard-facing electrode and then notched. The specimen was cooled to the desired temperature and was impacted by a dropped weight on the reverse (unwelded) side in order to initiate a brittle crack running from the notched weld into the base metal. The impact energy is specified depending on the material's yield strength: 350 J for σ_y up to 410 MPa and 400 J for σ_y between 410 MPa and 620 MPa. A "no-break" result is where a brittle crack initiates but does not spread across the full width of the specimen i.e. it initiates and is arrested. If the crack spreads at least across the full width of the specimen, then it was considered to be a "break" result. The test was repeated at a range of temperatures to find the NDTT, which is the highest temperature at which the specimen shows a "break" result i.e. all specimens at temperatures above this show "no-break" results.

Table 3
Summary of tensile properties of the steels considered in this research. Uncertainty is taken as two standard deviations of the results.

	M01	M02	M03	M04	M05	M06
Material	RPV A543	RPV A302	X65	S355 G10 + M	S355 G10 + M	EH47
Thickness (mm)	28	28	30	90	50	80
Average E (GPa)	233 ± 16	227 ± 15	188 ± 5	208 ± 66	217 ± 24	270 ± 112
Average UTS (MPa)	845 ± 31	740 ± 17	613 ± 21	509 ± 2	536 ± 12	622 ± 15
Average σ_y (MPa)	756 ± 34	601 ± 13	566 ± 17	386 ± 4	444 ± 32	490 ± 10
Average RoA (%)	73 ± 4	66 ± 2	81 ± 2	77 ± 1	83 ± 1	78 ± 5
STRA Average UTS (MPa)	835 ± 18	733 ± 7	595 ± 5	501 ± 2	512 ± 1	618 ± 3
STRA Average RoA (%)	57 ± 6	55 ± 4	81 ± 3	75 ± 4	77 ± 5	79 ± 1

Furthermore, instrumented Charpy V notch (CVN) tests were carried out at a range of temperatures, following BS EN ISO 148-1 [63], to determine the ductile to brittle transition curve and upper shelf absorbed energy which is commonly used in industry to estimate fracture toughness. Instrumented Charpy tests differ from traditional Charpy tests by measuring the force on the hammer throughout the test as well as the absorbed energy. The post-fracture force, also known as the arrest force, was extracted for each specimen which showed arrest behaviour. This data was analysed to determine at what temperature the post-fracture force would be 4 kN, T_{4kN}.

Tensile testing was carried out on all materials under two different conditions. Traditional tensile tests following BS EN ISO 6892 [64] were carried out to determine the yield strength and ultimate tensile strength (UTS) of the materials along with the ductility which was taken as the reduction of area (RoA) or elongation in this work. Additionally, alternative tensile tests, "short transverse reduction of area" (STRA) tests were carried out to measure the ductility in the through-thickness direction following BS EN 10164 [65]. This was done to investigate whether the ratio of ductility between the rolling axis and through-thickness axis can be used as a proxy for the material's texture, which is believed to influence crack arrestibility [66,67].

For the microstructural analysis, optical microscopy was carried out on all materials. The specimens were mounted, polished, and etched with 2% nital solution to reveal the grain boundaries. In order to best consider the range of microstructures present throughout the thickness of the materials, the grain size analysis was carried out at the quarter wall location on the plates. It was decided to measure the grain size for each steel by the linear intercept method, following ASTM E112 [68], because the grains did not appear to be equiaxed. This method reports the grain size as the average grain diameter which is the geometric mean of the average grain diameter in each of the principal directions. In order to determine the grain aspect ratio, the grain sizes were measured in each of the three orthogonal directions of the plate; rolling direction, through thickness direction, and perpendicular to the rolling direction.

Finally, Single Edge Notched Bend, SEN(B), fracture toughness testing was done on each material, following BS 7448-1 [69], to quantitatively determine the fracture toughness as the maximum crack tip opening displacement (CTOD δ_m). The testing was carried out at a temperature on the upper shelf as determined by the Charpy testing so that they can be compared to the upper shelf CVN energy for the material. Typically this was room temperature for most of the steels. In addition to testing all of the steels at their upper-shelf temperatures, half of the steels (M01, M02 and M06) had fracture toughness tests carried out at temperatures within the transition temperature and lower shelf, to help support discussions about crack arrest predictions based on the Master Curve. The SEN(B) specimen geometries are summarised in Table 1, and each specimen had an initial crack length, a_0, of 0.5 W (i.e. 10 mm). The specimens were not side grooved as this is not necessary for small sized specimens like the ones employed in the present study.

4. Test materials

4.1. Selected materials

The test programme in this study was carried out on five materials, in six batches, which are summarised in Table 2; 1- reactor pressure vessel (RPV) A543 steel with the thickness of 28 mm (denoted M01), 2- RPV A302 steel with the thickness of 28 mm (denoted M02), 3- X65 pipeline steel with the thickness of 30 mm (denoted M03), 4- S355G10 + M

Table 4
Summary of chemical composition of the steels considered in this research.

	M01	M02	M03	M04	M05	M06
C	0.17	0.19	0.04	0.07	0.06	0.05
Si	0.38	0.31	0.18	0.27	0.35	0.22
Mn	0.3	1.47	1.63	1.57	1.54	1.41
P	0.007	0.012	0.006	0.013	0.012	0.01
S	0.005	0.004	<0.002	<0.002	<0.002	0.005
Cr	1.49	0.23	0.17	0.035	0.16	0.21
Mo	0.46	0.52	0.12	0.007	0.013	0.25
Ni	2.95	0.59	0.48	0.34	0.032	0.78
Al	0.014	0.012	0.027	0.032	0.035	0.039
As	<0.004	<0.004	<0.004	<0.004	<0.004	<0.01
B	<0.0005	<0.0005	<0.0005	<0.0005	<0.0005	<0.003
Co	0.008	0.006	<0.004	<0.004	<0.004	<0.01
Ceq (IIW) [73]	0.81	0.62	0.40	0.36	0.35	0.43

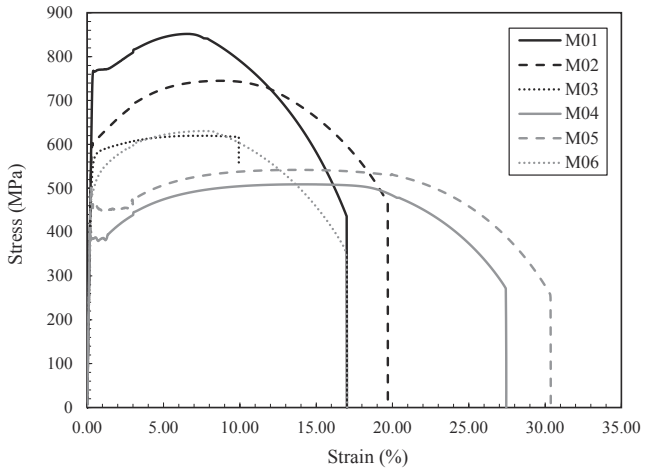

Fig. 1. Tensile curves for all six materials used in this study.

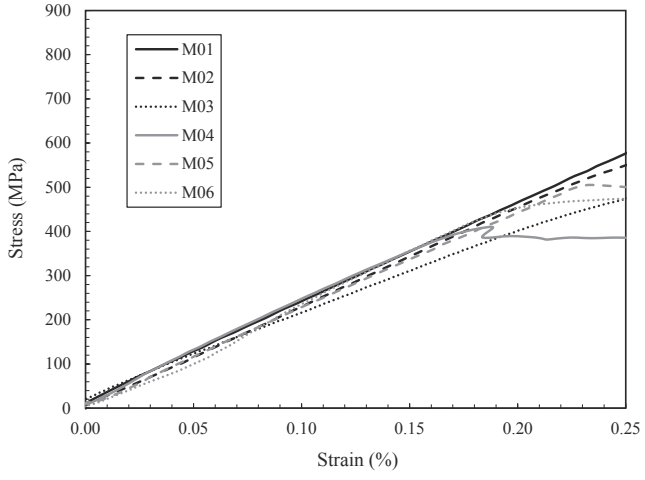

Fig. 2. Young's modulus region of tensile curves for all six materials used in this study.

structural steel plate with the thickness of 90 mm (denoted M04), 5- S355G10 + M structural steel plate with the thickness of 50 mm (denoted M05), and 6- EH47 shipbuilding steel with the thickness of 80 mm (denoted M06). The materials selected in this study are widely used in offshore Oil & Gas, nuclear power plants and offshore wind applications, therefore the obtained results and drawn conclusions from this research are expected to have a significant impact on design and life assessment of engineering components and structures employed in a wide range of industries.

4.2. Mechanical properties – Tensile (roundbar and STRA) and chemical

The tensile and chemical properties of the materials considered in this study are given in Tables 3 and 4, with an example tensile curve for each material given in Fig. 1 and the Young's modulus region emphasised in Fig. 2. The wide variation in yield stress, σ_y, and the UTS between the different materials is evident in Table 3. Materials M04 and M05 (both nominally S355 structural steels) are an excellent example to demonstrate the variation in "off-the-shelf" steels. They were the same steel grade and produced through the same manufacturing route, however they show a difference in mechanical properties and chemical composition. This is common for steels because the standard grades allow for a great deal of flexibility [70]. It is worth noting that there is generally low scatter for most of the tensile test results between the 3 specimens of each material although due to the low number of specimens tested, the scatter is of low statistical significance. However, materials M04 and M06 show high scatter in their elastic modulus results. For M04 this is due to one much lower result of 171GPa and for M06 there was one much higher result of 334GPa which is quite an unexpected and extreme value. This kind of scatter in elastic modulus is common for steels and may be due to local inhomogeneities in the material which were picked up during the small sample size of the tensile specimen or minor inconsistencies in test procedure [70–72]. Generally, both the UTS and reduction of area (RoA) were lower in the STRA test (i.e. through thickness direction) as opposed to the tensile tests along the rolling direction. However for materials M03 and M06, the RoA was the same between the two orientations.

As seen in Fig. 1, there is generally negative trend between strength and ductility, with the highest strength steel, M01, having a low strain at failure and the lowest strength material, M05, having the highest strain at failure. However, this trend is not consistent for all the steels, for example material M03 which has an intermediate strength but a very low strain at failure. The increased strain at failure for materials M04 and M05 may be due to their low carbon equivalent content which contributes to a higher ductility. As seen in Tables 3 and 4, the RPV steels (M01 and M02) have the highest carbon and carbon equivalent content in comparison to the other steels, hence higher yield stress values were observed in RPV steels. Further comparison between the chemical composition of the steels show that there is a variation in Mn and Cr contents: for example, M01 has a far smaller Mn content than the other five batches of steel, which is replaced by a greater Cr and Ni content. Apart from these points of note, the steels have relatively similar compositions. The other variations in tensile properties are likely to be due to microstructural differences between the steels such as their grain size, grain orientation and phase structure.

4.3. Microstructure analysis

The micrographs of all six batches of steels considered in this study after polishing and etching is shown in Fig. 3. The examined slices were extracted from mid-thickness of each batch of material. In Fig. 3, X indicates the rolling axis and Z indicates the through thickness axis. The micrographs show the variability in carbon contents for each of the materials, with carbide and pearlite regions evident in M01 and M02 which had the greatest carbon contents than the other materials, which show more pure ferritic regions. In these micrographs, the grains appear to be elongated along the rolling direction, which is investigated through grain size analysis. The average grain size measured for each steel, which is the combined average, is summarised in Table 5. As seen in Table 5 and Fig. 3, the largest and smallest average grain size has been found in RPV A543 (M01) and EH47 (M06), respectively.

Fig. 4 correlates the aspect ratio of ductility (using RoA) against the

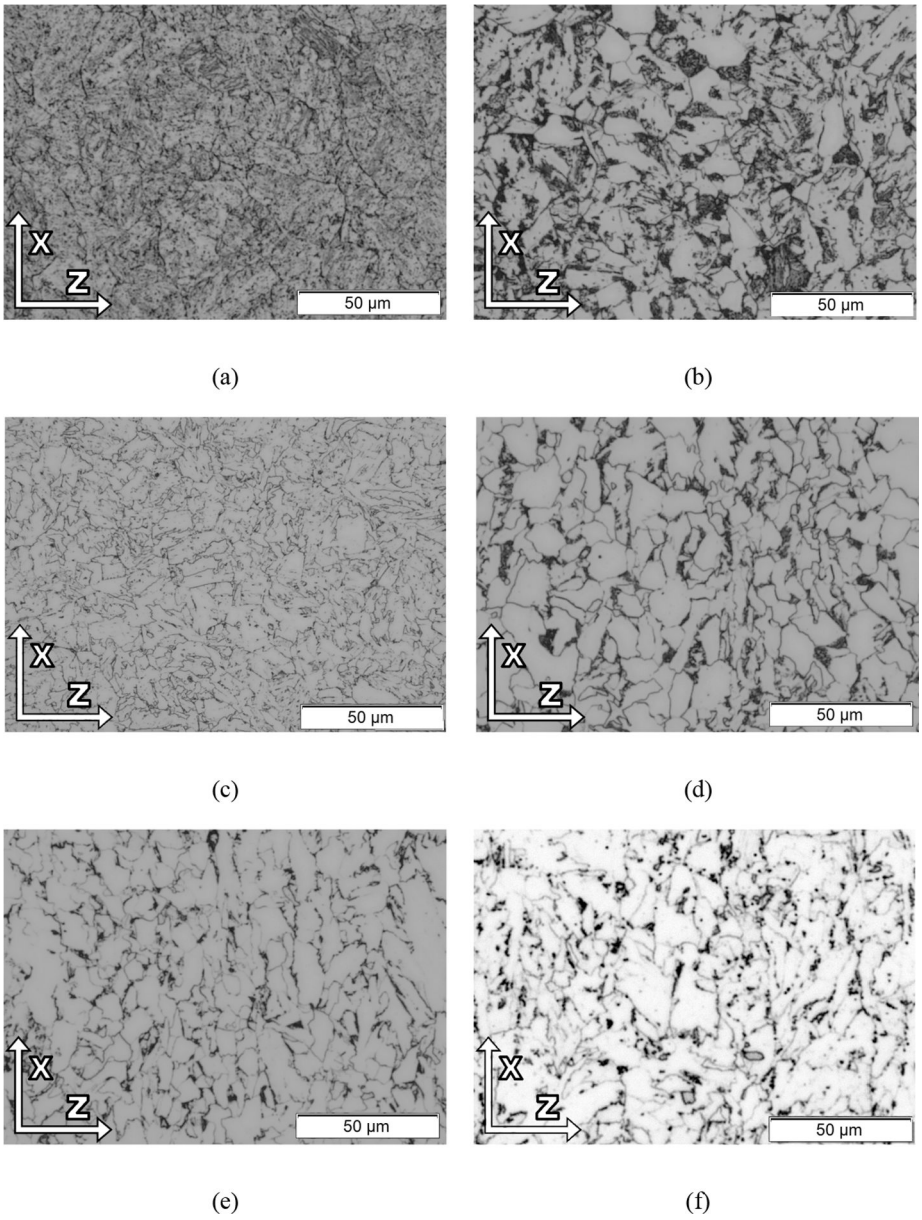

Fig. 3. Microstructure of (a) M01, (b) M02, (c) M03, (d) M04, (e) M05, and (f) M06 steels.

Table 5
Grain sizes of the steels used in this study (measured to ASTM E112).

	M01	M02	M03	M04	M05	M06
Average Grain Size (μm)	9.5 ± 1.4	7.0 ± 1.2	5.2 ± 1.3	5.6 ± 0.9	7.5 ± 0.9	4.1 ± 0.5

aspect ratio of grain size: these values are the ratio of the RoA (or average grain size) along the rolling axis and that along the through-thickness axis. If the anisotropy of the material's tensile properties is due to elongated grains in a certain direction, then this ratio would be expected to follow a 1:1 trend. However, the results showed a direct negative correlation, and a significant offset from the origin, which indicates that bulk measures of anisotropy cannot necessarily identify microstructural grain elongation. Other microstructural factors that can contribute to a steels' macroscopic behaviour might include the size and distribution of inclusions, and centreline segregation, which have not been included in the microstructural consideration here. Further analysis of the grain aspect ratio in Fig. 5 shows that there is no strong correlation between grain size and the aspect ratio, although as these steels are all very finely grained and there is not enough variation between them to make a firm conclusion.

5. Experimental results from small-scale tests

5.1. Instrumented Charpy V notch impact test results

The key results from the instrumented CVN tests are shown in Table 6, with the fit to the Charpy curve for each material shown in Fig. 6. It is evident that material M02, one of the RPV steels, is designed for use at elevated temperatures as the transition for this material occurs well above room temperature. The other steels show a wide range of upper shelf CVN energy values, but their transition region (with varying slopes) lies in the same window of around −100 °C to −50 °C, making them suited to work at ambient temperatures. Material M03 has the highest upper shelf Charpy energy, followed by materials M05 and M06 which both have almost the same upper shelf Charpy energy. Despite being the same steel grade as M05, M04 has a markedly lower upper

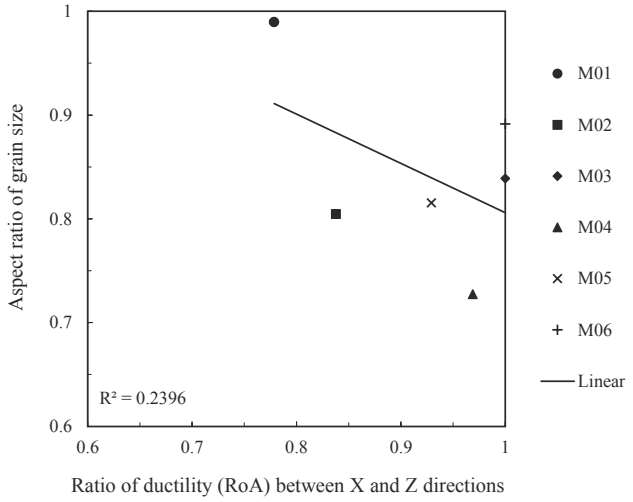

Fig. 4. Correlation between grain size aspect ratio and ratio of ductility in the rolling direction.

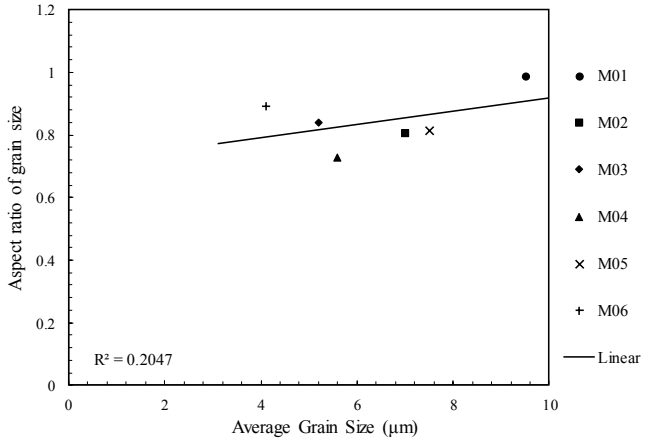

Fig. 5. Correlation between average grain size and grain aspect ratio in the rolling direction.

Table 6
Summary of Charpy results for each material, including reference temperatures.

	M01	M02	M03	M04	M05	M06
CVN Upper Shelf (J)	122	140	410	210	295	297
T_{4kN} (°C)	−100	14	−90	−113	−112	−156
CVN T_{27J} (°C)	−117	−13	−72	−102	−113	−115

shelf Charpy energy and although they had the highest tensile strength, the RPV steels have the lowest upper shelf Charpy values of any of the materials. The reference temperatures given in Table 6 will be discussed later, but suffice to say that there seems to be no relationship between a material's T_{4kN} and its T_{27J} – for example for materials M03, M04 and M06 the T_{27J} is notably higher than the T_{4kN}, however a reverse trend is seen for materials M01 and M02 and no difference is seen between the two for material M05.

5.2. Pelini test results

The Pellini test results are summarised in Table 7, with the full results given in Fig. 7. In this figure, the open white points indicate that a fracture event occurred at this temperature and the solid black points indicate that no fracture event occurred at this temperature. At some

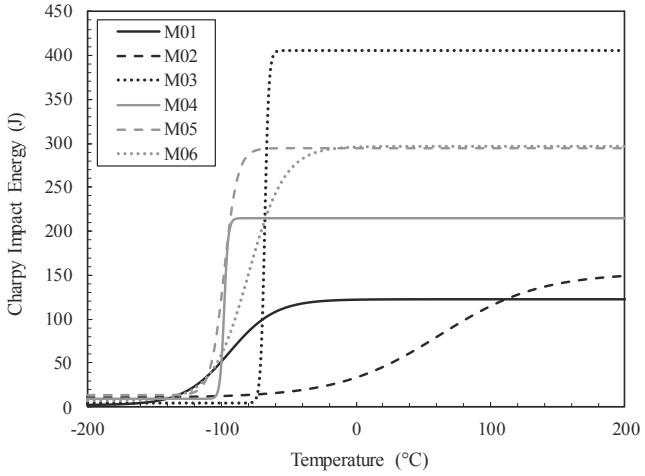

Fig. 6. Charpy curve for each material given as a tanh fit to the data.

Table 7
Summary of NDTT values determined through Pellini testing.

	M01	M02	M03	M04	M05	M06
NDTT	−75 °C	20 °C	−30 °C	−50 °C	−60 °C	−50 °C

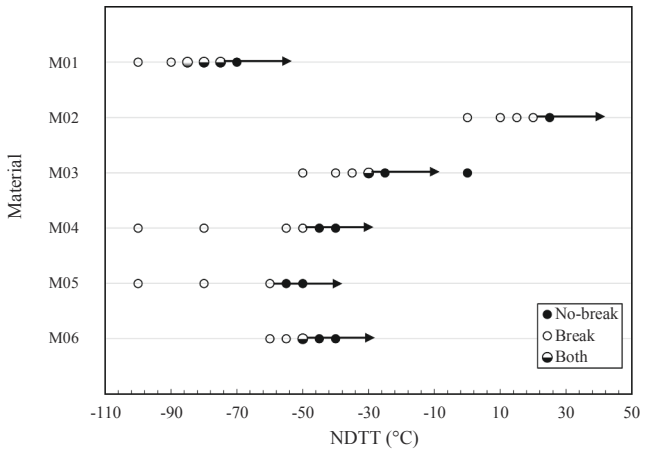

Fig. 7. Pellini test results for each material.

temperatures, both "break" and "no-break" results occurred, and these are indicated with a mix of the two symbols. The arrows indicate the temperature above which no fracture event occurred– i.e. the crack was arrested and it is above the NDTT of the material. A low NDTT indicates good brittle crack arrestibility for that material.

The two RPV steels, M01 and M02 had the lowest and highest NDTT values respectively. Intermediate NDTT values were seen for the other steels, with material M03 having a slightly higher value followed by materials M04 and M06, and material M05 having a slightly lower value. These results show some similarities with the Charpy results in that materials M01 and M06 had shallower Charpy transition curves than the other materials and here they show some temperatures with both break and no-break results which indicates a wide transition region. However, material M02 which had a shallow Charpy transition curve showed very well defined Pellini behaviour which indicates a narrow transition region and shows disagreement with the Charpy curve.

Table 8
Summary of results from upper shelf fracture toughness testing. RT indicates room temperature.

	M01	M02	M03	M04	M05	M06
Test Temperature	RT	120C	RT	RT	RT	RT
Average CTOD δ_m (mm)	0.40	0.36	0.86	1.15	1.40	0.86

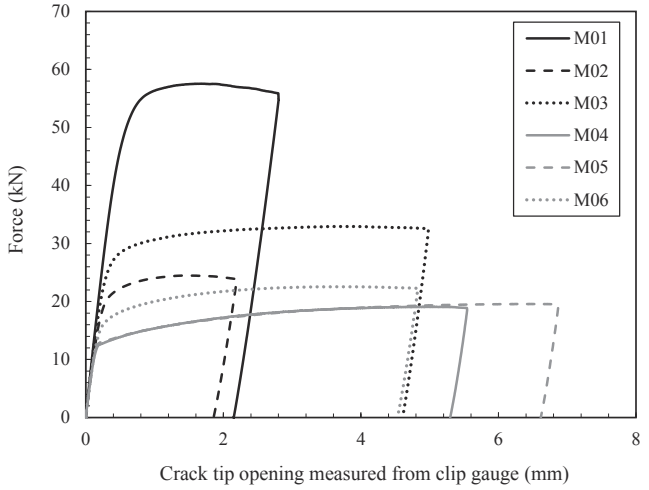

Fig. 8. Force against CTO plots for each of the materials.

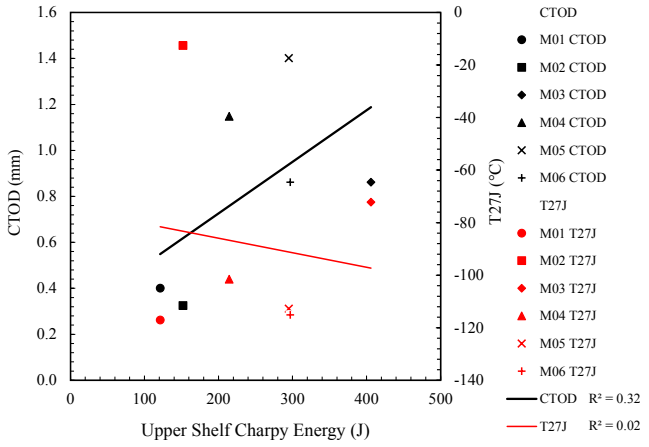

Fig. 9. Correlation between initiation toughness parameters; CTOD δ_m and T_{27J} with upper shelf Charpy energy.

5.3. SEN(B) fracture toughness test results

The materials' CTOD δ_m results are summarised in Table 8, with an example force vs. crack tip opening (CTO) curve for each material given in Fig. 8. The CTOD δ_m results are calculated from the CTO at which the maximum force is observed using the procedure given in BS 7448-1. This procedure involves using the area under the force/CTO curve along with the specimen dimensions and the material properties in order to calculate CTOD δ_m. It can be seen that the highest CTOD δ_m is found in material M05, followed by material M04 and then by materials M03 and M06. The lowest CTOD δ_m was found in materials M02 and then M01, which had similar results. These results are mirrored in the Force/CTO traces which show the same trend of maximum CTOD δ_m for the materials. Additionally, there seems to be a correlation between high CTOD δ_m and low tensile strength. M01 and M02 had the highest UTS values and show the lowest CTOD δ_m, M03 and M06 show the mid range for

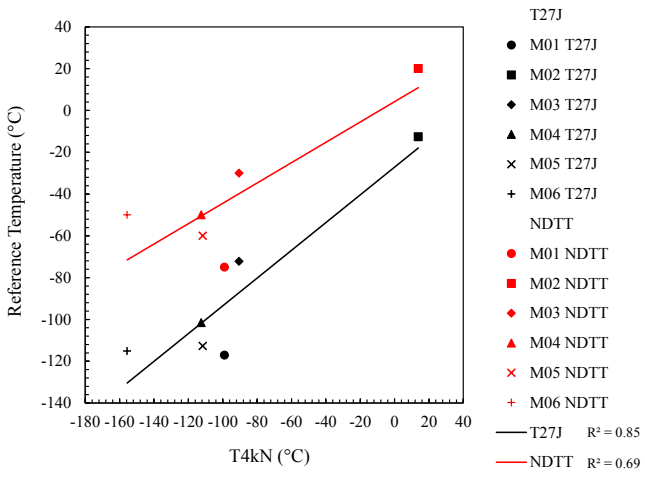

Fig. 10. Correlation between arrest toughness reference temperatures; T_{27J} and NDTT with T_{4kN}.

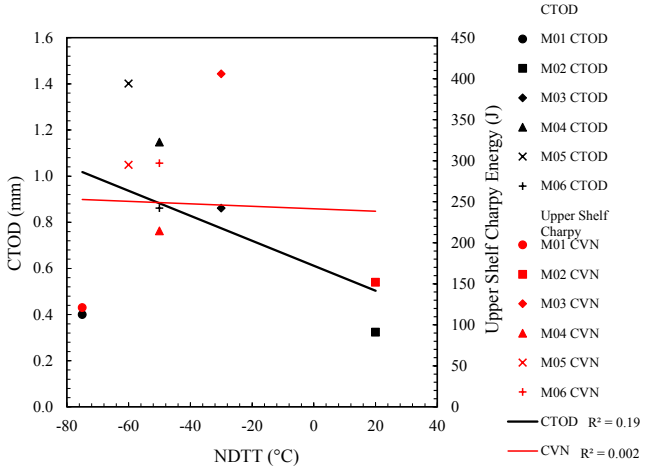

Fig. 11. Correlation between fracture initiation toughness and crack arrest toughness parameters; CTOD δ_m and upper shelf Charpy energy with NDTT.

both properties, and M04 and M05 show the highest CTOD δ_m and the lowest UTS results. Although their material properties have shown differences, it is noticeable that the traces for materials M04 and M05, nominally the same steel grade, overlap. This indicates that they are showing a similar response to fracture, although material M05 has the higher overall toughness. Another notable difference between these materials is the amount of force needed to reach the maximum CTO, with material M01 requiring a large force to reach a relatively low CTOD δ_m compared to material M02, which has a similar CTOD δ_m but took much less force to reach this point.

6. Discussion

6.1. Correlation between the obtained fracture parameters

The results from fracture toughness and Charpy impact tests are presented and compared with each other in Figs. 9–11. The correlation between initiation toughness parameters, CTOD δ_m and T_{27J}, with upper shelf Charpy energy has been investigated in Fig. 9. As seen in this figure, there is a weak linear correlation between upper shelf Charpy energy and CTOD δ_m fracture toughness, excluding M03, which has the highest Charpy energy, but the median fracture toughness compared to the other materials. But overall, the results in Fig. 9 suggest that an increase in the upper shelf Charpy energy results in an increase in CTOD

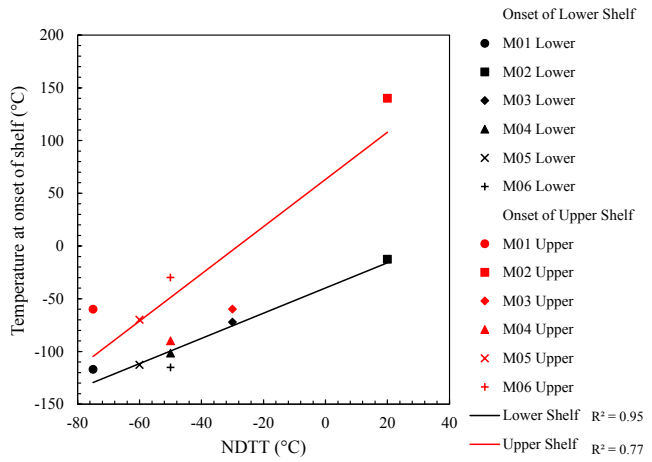

Fig. 12. Correlation between arrest toughness parameter NDTT and transition temperatures for both the upper and lower shelf of the Charpy transition curve.

δ_m as there is a loose linear correlation between these two parameters ($R^2 = 0.32$). On the other hand, it is evident from this figure that there is no correlation between the upper shelf Charpy energy and the lower shelf temperature, T_{27J}, as the regression line between these two parameters shows almost no correlation ($R^2 = 0.02$).

The possible correlation between arrest toughness reference temperatures, T_{27J} and NDTT, with T_{4kN} has been investigated and the results are shown in Fig. 10. It can be observed in this figure that there is a good linear correlation ($R^2 = 0.69$) between parameters indicating arrestibility, NDTT and T_{4kN}, determined through Pellini and Charpy tests. Also seen in this figure is that T_{4kN} shows a strong correlation with the onset of the lower shelf, T_{27J} ($R^2 = 0.85$). Comparing the lines of best fits to the data points in Fig. 10 it can be seen that within the inherent experimental scatter, the slope of the line of best fit made to T_{27J} data is slightly steeper than the NDTT data, when the results are correlated with T_{4kN}.

The CTOD δ_m and upper shelf Charpy energy results are plotted against NDTT data in Fig. 11. As demonstrated by Fig. 11, the arrest parameter, NDTT, does not correlate with the fracture initiation toughness parameters when the results from all six batches of steels considered in the analysis. As an example, material M01 has the lowest NDTT and T_{27J} of all the steels, which indicates a high arrestability. However this material has the smallest Charpy toughness of any of the materials. Although M02 has approximately the same Charpy toughness as M01, it has the highest NDTT and T_{27J} which indicates very poor arrestibility. This example shows how concerning it is that modern steels can be judged based on their Charpy toughness (which is measured on the upper shelf) although this may not indicate their arrest properties.

Since brittle crack arrest properties are heavily dominated by the lower transition region and lower shelf, it is important to investigate these parameters further. Figs. 12 and 13 relate the NDTT to each material's ductile to brittle transition curve. As the NDTT defines the onset of brittle behaviour, it would be expected to lie close to the T_{27J} temperature at the onset of the lower shelf of the Charpy curve. However the NDTT for each material is located on the upper transition or upper shelf of the Charpy transition curve, except for material M02 which shows the expected behaviour. In spite of this, the NDTT can be strongly correlated ($R^2 = 0.95$) against T_{27J}, i.e. as expected, the temperature at the onset of the lower shelf correlates strongly with that of the onset of brittle behaviour. Although this correlation was expected, it holds even for the materials which had their NDTT lie on the upper shelf or transition region of the Charpy curve. However, this correlation is much weaker when the NDTT is correlated against the temperature of the upper shelf, which is probably because the transition region for some of these materials is shallow and for others it is steep. There are concerns with the NDTT of some materials lying on the upper shelf of the Charpy curve because these materials are at a risk of behaving in a brittle manner at a higher temperature than is predicted from the Charpy transition curve. This is a concern because it means that a running brittle crack would not be arrested if it initiated, for example through accidental damage.

6.2. Correlation between mechanical properties and microstructure

The steels examined in this study all have small grain sizes, which makes it more complex to correlate the mechanical properties against the microstructural characteristics due to the cluster of grain size values giving high uncertainty. Fig. 14 shows that the average grain size correlates loosely against the upper shelf Charpy energy, and very weakly against the CTOD δ_m fracture toughness. It is well-accepted that grain refinement provides improved tensile properties and initiation fracture toughness for steels and this is likely to be the reason why these steels are designed to have very fine grain sizes on average. Although only a weak correlation, this observation is consistent with the results presented in the open literature by other researchers[74–76].

The grain size and aspect ratio are plotted against NDTT in Fig. 15. It can be seen in this figure that no strong correlations can be made between the average grain size or aspect ratio of grain sizes and the material's arrest properties when all six batches of steels are considered in the analysis. However, by excluding the largest value of NDTT, which is associated with material M02, the overall trends indicate an increase in NDTT with a reduction in grain size and aspect ratio with the average grain size having a more pronounced effect (i.e. steeper trend) on the NDTT results. This would mean that a smaller grain size gives poorer brittle crack arrest properties than a larger grain size, which contradicts the observations seen on the relationship between grain size and initiation toughness. This is in agreement with recent results from other researchers [9]. Additionally, the grain aspect ratio does not seem to affect the arrest parameter NDTT significantly. The microstructural grain anisotropy has not been shown to be a factor in the crack arrest behaviour on its own, and other factors such as composition, inclusion size and distribution, plate centreline and surface microstructures, might also be influential.

The aspect ratio due to elongation of the grains along the rolling axis was estimated from the material's bulk ductility, in terms of tensile properties, which was correlated against the measured grain size aspect ratio. The observations showed a direct negative correlation. It would be expected that if the material was isotropic (i.e. tensile properties are identical along each axis), the grains would be equiaxed and not show elongation along the rolling axis. However, these steels showed the opposite behaviour. M01 had the most uniformly shaped grains, but had the greatest decrease in ductility in the through-thickness direction. Similar behaviour was seen for the other steels, which could be caused by the materials' texture, distribution of inclusions, grain structure or test procedure.

6.3. Comparison of the experimental results with empirical predictions

The relationship between NDTT and T_{27J} shown in Fig. 12 is not 1:1, which means that Eqs. (1)–(3) cannot be considered valid for modern steels, and using these equations results in over-predicting the NDTT in almost every case, which is shown in Fig. 16. For the materials studied here, there is an offset between the NDTT and T_{27J} of approximately 40 °C ± 10 °C, which is similar to Eq. (4) and the offset between the NDTT and CAT. It is recommended that the CAT is measured through large-scale crack arrest testing to determine the validity of these predictions, but it can be seen that the reference temperatures do indeed show strong agreement with each other. It is recommended to carry out Pellini tests to determine the NDTT of the material rather than relying on Charpy data.

The master curve method given in Eqs. (8)–(10) gives the predicted lower bound toughness shown in Fig. 17 using M06 as an example. In

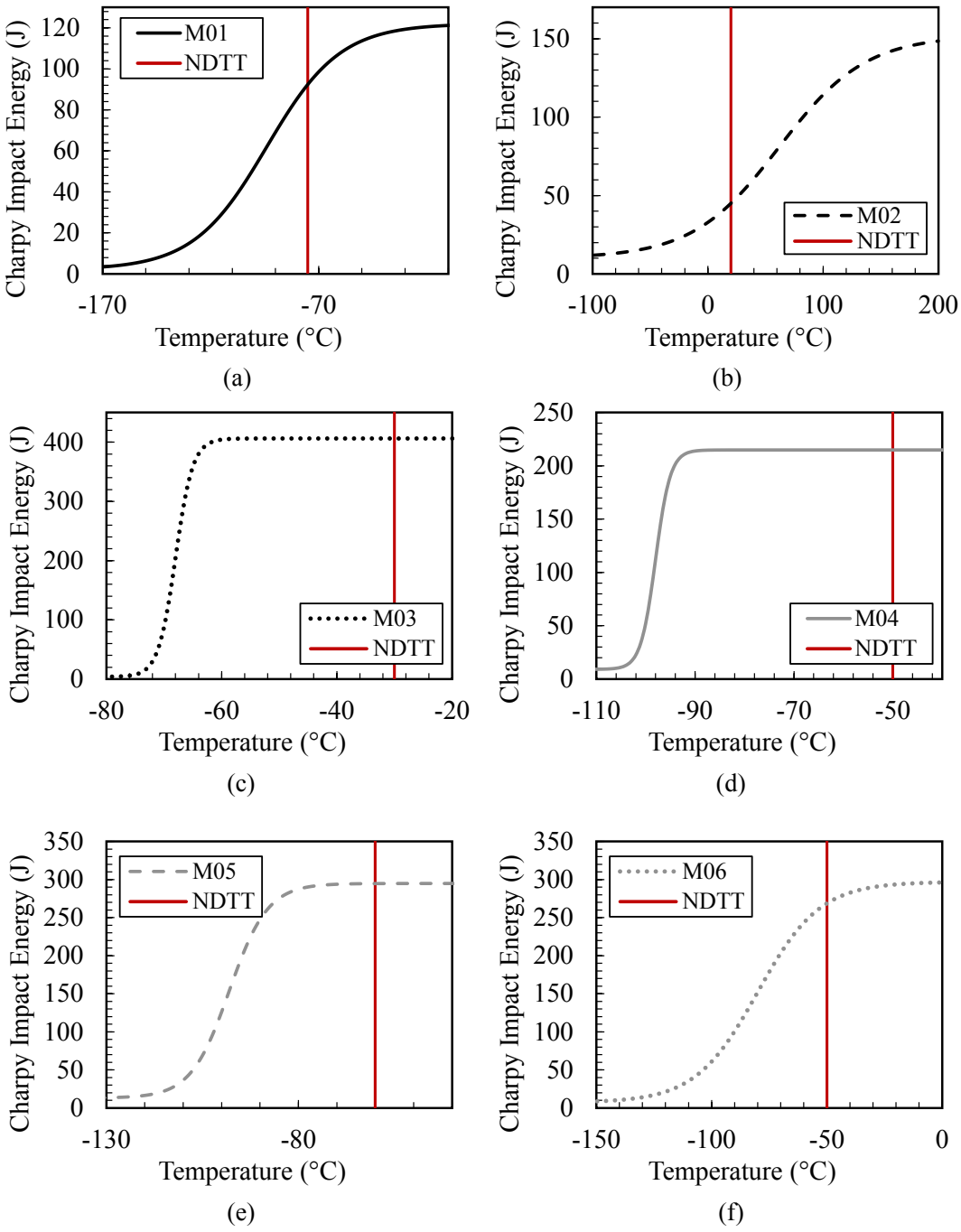

Fig. 13. The location of the NDTT on the Charpy transition curve for (a) M01, (b) M02, (c) M03, (d) M04, (e) M05, and (f) M06 steels.

order to give an indication of the accuracy on these relationships, additional SEN(B) tests were carried out at low temperature between −50 °C and −120 °C and the results are in good agreement with the K_{IC} prediction from the master curve approach at low temperatures. However, as expected, the agreement is limited to the lower end of the transition region and agreement is poor at −50 °C. The prediction based on T_{4kN} gives a toughness prediction similar to the K_{IC} until −50 °C, the NDTT, where they diverge. A more conservative prediction of K_{Ia} is given by the prediction from NDTT, which indicates that the NDTT gives a conservative prediction of the materials' toughness compared to using the Charpy energy. For brevity, master curves for other materials are not shown here but can be found in Appendix B. Generally, for the other materials, K_{Ia} prediction from NDTT gave the most conservative toughness estimate. Low temperature SEN(B) fracture toughness tests on materials M01 and M02 show a similar trend of good agreement on the lower shelf and lower transition, and poor agreement in the upper transition region. This is a limiting factor on the use of these predictions at ambient temperatures.

7. Conclusions

In this work, a wide range of mechanical testing, including grain size measurements, was carried out on 6 different batches of structural steels to investigate the relationship between mechanical properties and microstructure with respect to fracture initiation and brittle crack arrest. The following key conclusions have been drawn from the present study:

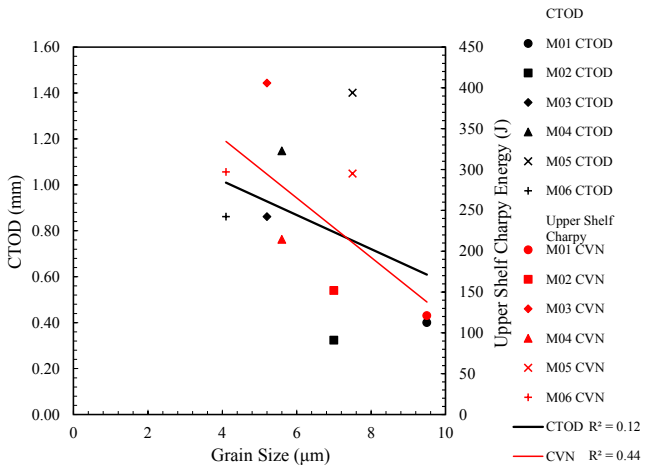

Fig. 14. Correlation between grain size and initiation toughness parameters; CTOD δ_m and upper shelf Charpy energy.

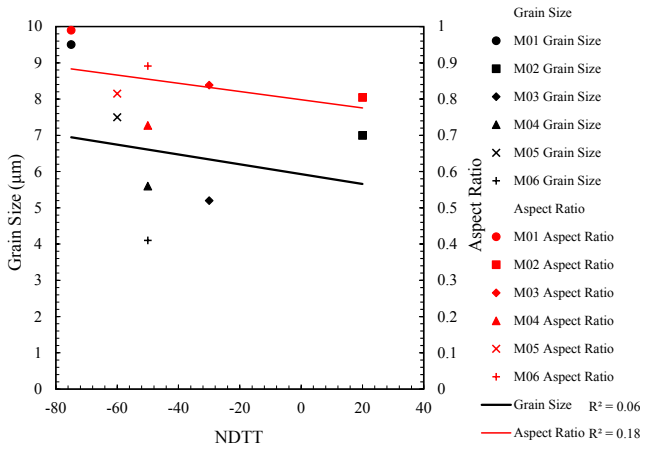

Fig. 15. Correlation between arrest toughness parameters and microstructural characteristics; average grain size and grain aspect ratio with NDTT.

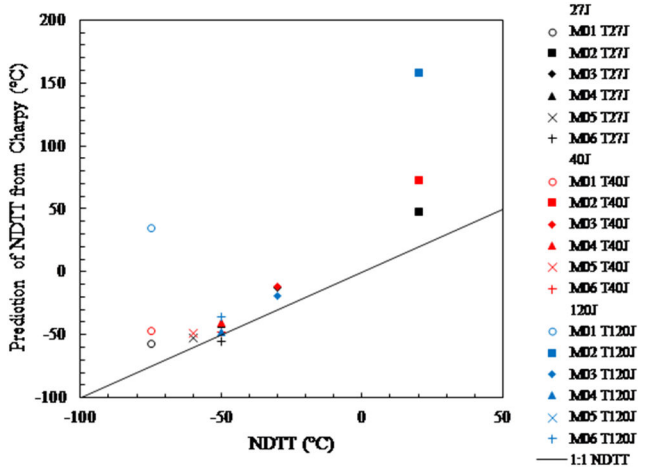

Fig. 16. Prediction of NDTT from Charpy reference temperatures.

- Improved fracture initiation behaviour of a steel (i.e. high CTOD δ_m and upper shelf Charpy toughness) correlates with a smaller average grain size, but crack arrest behaviour does not.

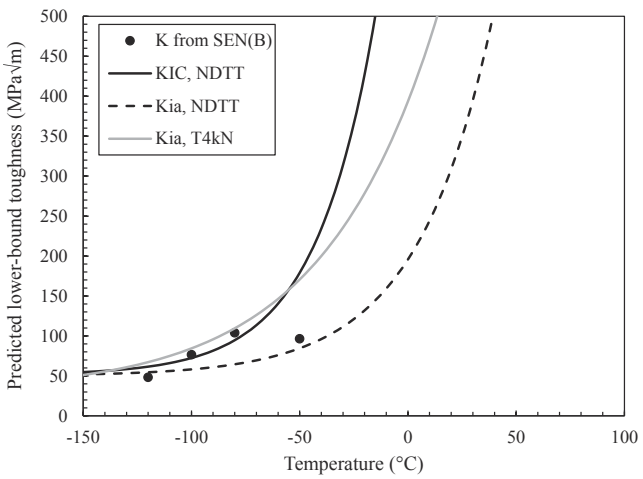

Fig. 17. Master curve predictions of toughness at a range of temperatures for M06.

- High CTOD δ_m fracture toughness or upper shelf Charpy energy does not indicate whether a material is protected from unstable brittle fracture because this is independent from high crack arrest toughness.
- For modern steels, the criteria that result in good crack arrest properties are not the same as those which result in a high upper shelf initiation fracture toughness. Therefore it is suggested to avoid using upper shelf fracture toughness parameters such as CTOD δ_m and Charpy energy to indicate crack arrestibility of modern steels due to poor correlation.
- The crack arrestibility of a material is most strongly correlated with reference temperatures based on the onset of brittle behaviour (such as T_{27J} and T_{4kN} from Charpy tests or NDTT from drop wright Pellini tests) – even for a steel where the NDTT is located at a temperature on the upper shelf of the Charpy transition curve.
- Master curve predictions of KI_a are more conservative when using NDTT than T_{4kN} so using the NDTT is recommended to give a safer estimate of crack arrest properties, although this prediction is only valid at low temperatures.
- It is recommended to characterise the crack arrest properties of steels using lower shelf parameters such as Pellini or Charpy testing to determine NDTT, T_{4kN} from instrumented Charpy tests, or T_{27J}.

CRediT authorship contribution statement

Jessica Taylor: Conceptualization, Methodology, Formal analysis, Writing - original draft. **Ali Mehmanparast:** Supervision, Writing - review & editing. **Rob Kulka:** Writing - review & editing. **Philippa Moore:** Formal analysis, Writing - review & editing. **Li Xu:** Writing - review & editing. **Gholam Hossein Farrahi:** Writing - review & editing.

Declaration of Competing Interest

The authors declare that they have no known competing financial interests or personal relationships that could have appeared to influence the work reported in this paper.

Acknowledgments

The authors would like to thank AN Steel who kindly provided the EH47 shipbuilding steel used in this work and to Weihong He and Li Xu who arranged this. Thanks to TWI Ltd for providing data and test material for M01 to M03, and to Cranfield University for providing steels M04 and M05. Thanks to TWI Ltd for provision of labs for the mechanical testing and metallurgical investigation. This work was

supported by Industrial CASE grant EP/P510464/1 (reference 2002942) and grant EP/L016303/1 for Cranfield, Oxford and Strathclyde Universities, Centre for Doctoral Training in Renewable Energy Marine Structures - REMS (http://www.rems-cdt.ac.uk/), both from the UK Engineering and Physical Sciences Research Council (EPSRC).

This publication was made possible by the sponsorship and support of Lloyds' Register Foundation. The work was enabled through, and undertaken at, the National Structural Integrity Research Centre (NSIRC), a postgraduate engineering facility for industry-led research into structural integrity established and managed by TWI through a network of both national and international Universities. Lloyd's Register Foundation helps to protect life and property by supporting engineering-related education, public engagement and the application of research.

Appendix A. Specimen extraction plan

See Fig. 18.

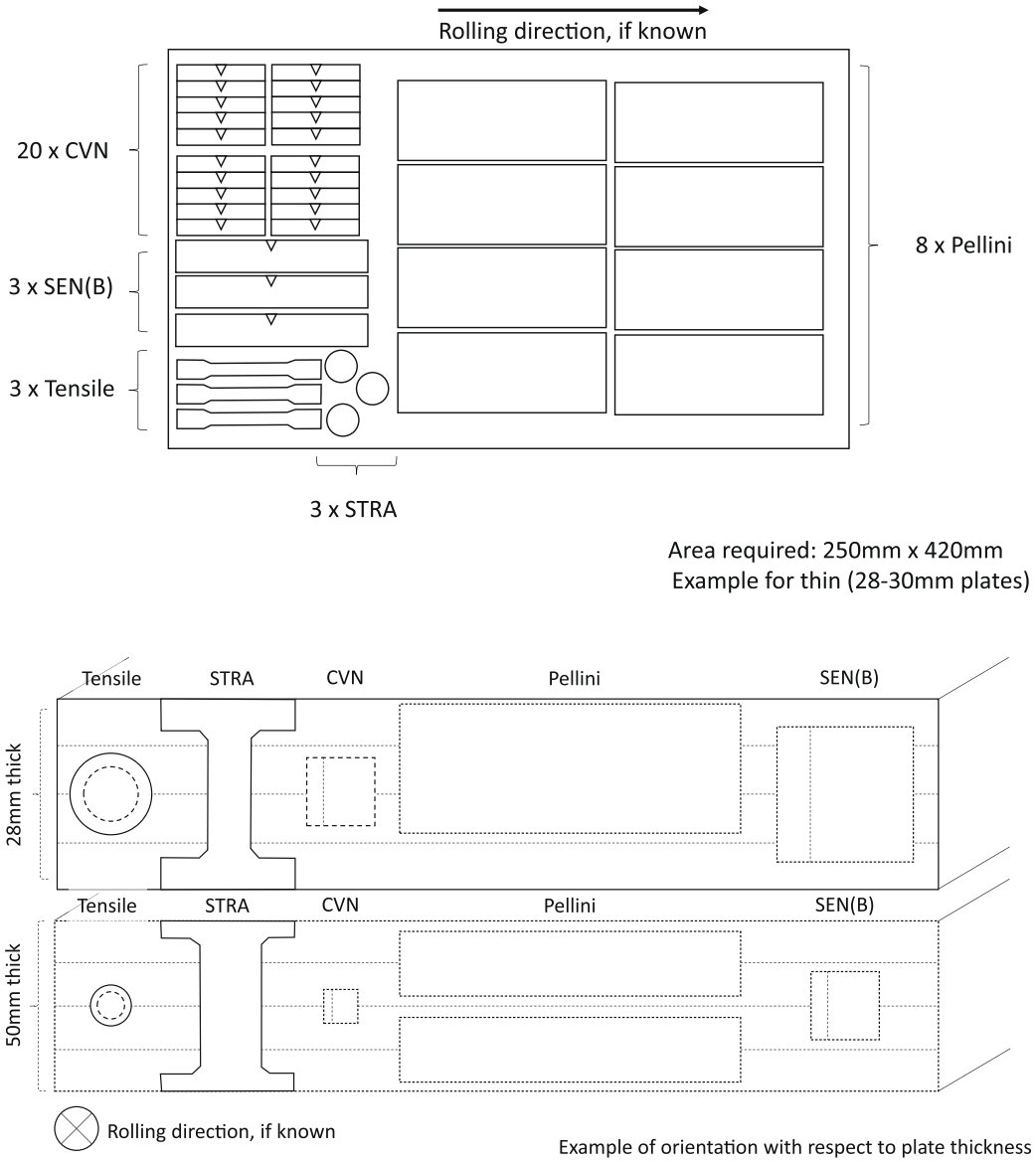

Fig. 18. Sectioning plan to show the specimen orientations with respect to rolling direction and plate thickness.

Appendix B. Master curves for all materials

See Figs. 19–24.

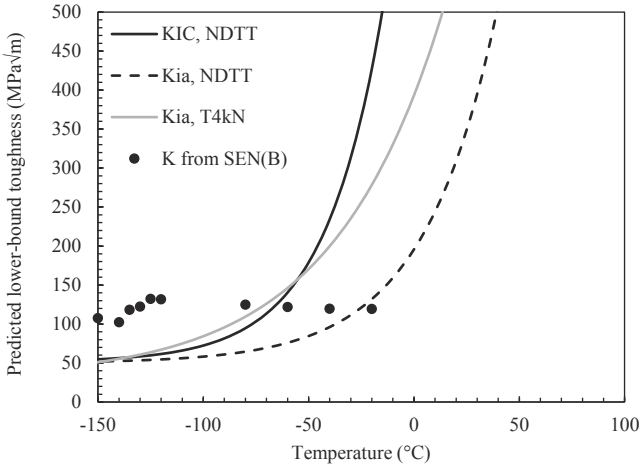

Fig. 19. Master curves for material M01.

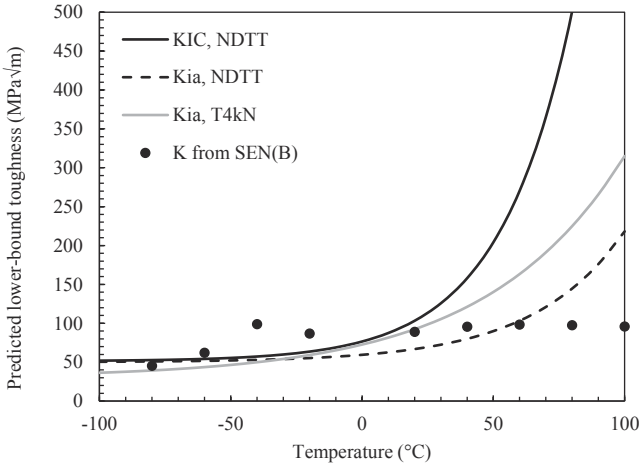

Fig. 20. Master curves for material M02.

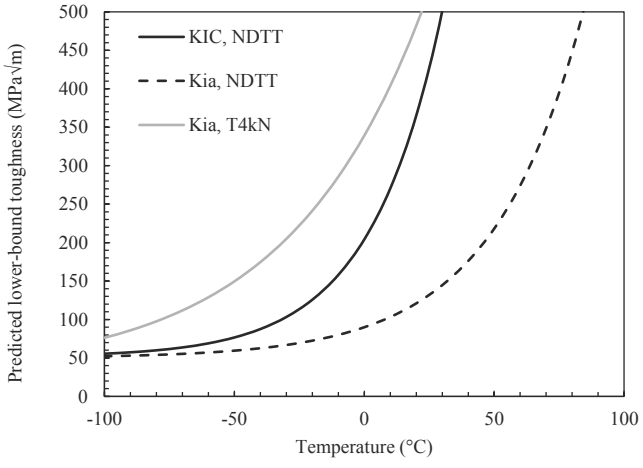

Fig. 21. Master curves for material M03.

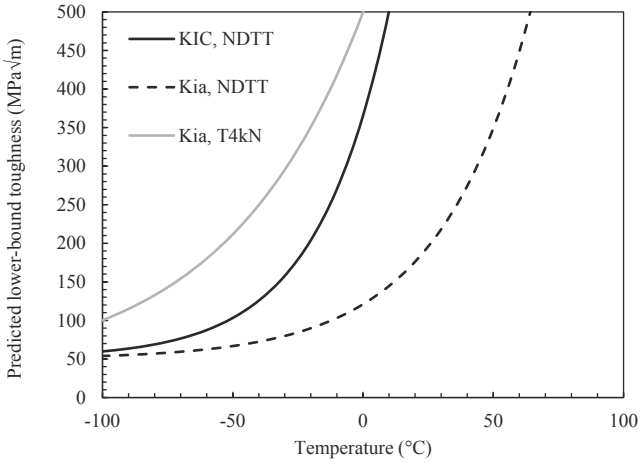

Fig. 22. Master curves for material M04.

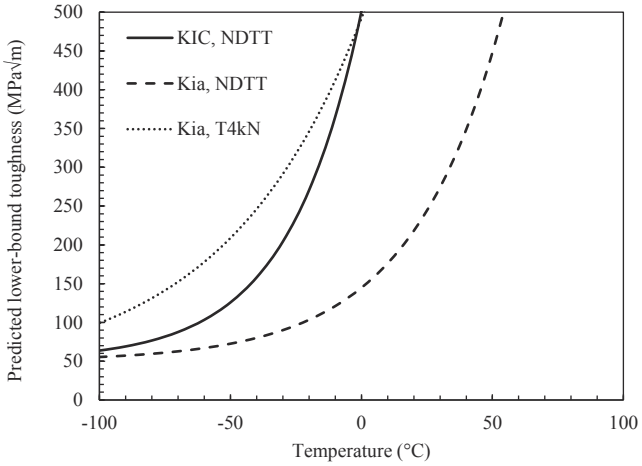

Fig. 23. Master curves for material M05.

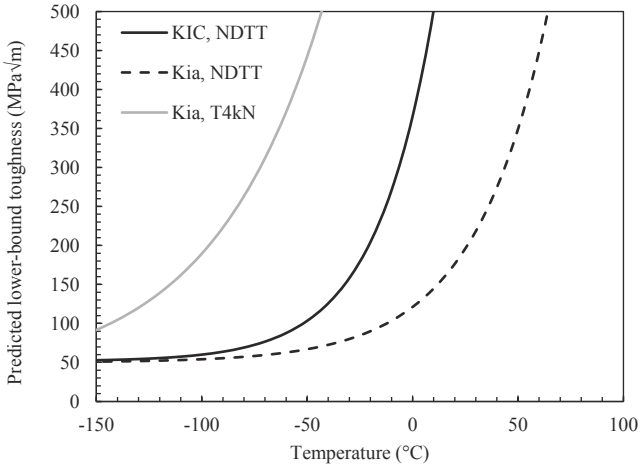

Fig. 24. Master curves for material M06.

References

[1] T.L. Anderson, Fracture Mechanics: Fundamentals and Applications, vol. 58, 2012, https://doi.org/10.1016/j.jmps.2010.02.008.
[2] (DNV) Det Norske Veritas, Fatigue Design of Offshore Steel Structures, Recomm Pract DNV-RPC203, Published online 2005.
[3] S.E. Hirdaris, W. Bai, D. Dessi, et al., Loads for use in the design of ships and offshore structures, Ocean Eng. (2014), https://doi.org/10.1016/j.oceaneng.2013.09.012.
[4] BS-7910, Guide to methods for assessing the acceptability of flaws in metallic structures, BSI Stand Publ. Published online 2013, https://doi.org/10.1007/s13398-014-0173-7.2.
[5] C. Wiesner, B. Hayes, A Review of Crack Arrest Tests, Models and Applications, 1995.
[6] A. Graville, Stress Analysis of Short Crack Arrest Test Report P244/1, Graville Associates Inc.
[7] P. Moore, G. Duncan, N. Singh, B. Bakthavathsalam, Comparing small-scale testing approaches to determine crack arrest in high strength steel, in: Proceedings Structural Integrity 2018, 2018.
[8] A. Völling, C. Kalwa, M. Erdelen-peppler, The misconception of employing cvn toughness as key-measure in ductile crack arrest prediction for modern line-pipe steels. Proceedings of the 2014 10th International Pipeline Conference IPC2014, 2014.
[9] F. Yanagimoto, T. Hemmi, Y. Suzuki, Y. Takashima, T. Kawabata, K. Shibanuma, Contribution of grain size to resistance against cleavage crack propagation in ferritic steel, Acta Mater. 177 (2019) 96–106, https://doi.org/10.1016/j.actamat.2019.06.038.
[10] M. Burdekin, W. Zhao, Y. Tkach, C. Wiesner, W. Xu, The Effects of Dynamic Loading on Structural Integrity Assessments, 2004.
[11] K. Shibanuma, F. Yanagimoto, T. Namegawa, K. Suzuki, Brittle crack propagation/arrest behavior in steel plate – Part I : Model formulation, Eng. Fract. Mech. 162 (2016) 324–340, https://doi.org/10.1016/j.engfracmech.2016.02.054.
[12] K. Shibanuma, F. Yanagimoto, T. Namegawa, K. Suzuki, Brittle crack propagation/arrest behavior in steel plate – Part II : Experiments and model validation, Eng. Fract Mech. 162 (2016) 341–360, https://doi.org/10.1016/j.engfracmech.2016.02.053.
[13] K. Shibanuma, F. Yanagimoto, K. Suzuki, S. Aihara, Brittle crack propagation/arrest behavior in steel plate – Part III: Discussions on arrest design, Eng. Fract. Mech. 190 (2018) 104–119.
[14] K. Shibanuma, F. Yanagimoto, T. Namegawa, K. Suzuki, S. Aihara, Modeling of brittle crack propagation/arrest behavior in steel plates in steel plates modeling high pressure turbine blade airplane gas turbine engine modeling of brittle crack behavior PCF propagation/arrest, Proc. Struct. Integr. 2 (2016) 2598–2605, https://doi.org/10.1016/j.prostr.2016.06.325.
[15] C. Berdin, M. Hajjaj, P. Bompard, S. Bugat, Local approach to fracture for cleavage crack arrest prediction, Eng. Fract. Mech. 75 (2008) 3264–3275.
[16] F. Yanagimoto, K. Shibanuma, K. Suzuki, T. Matsumoto, S. Aihara, Local stress in the vicinity of the propagating cleavage crack tip in ferritic steel, Mater. Des. 144 (2018) 361–373.
[17] A. Bousquet, S. Marie, P. Bompard, Propagation and arrest of cleavage cracks in a nuclear pressure vessel steel, Comput. Mater. Sci. 64 (2012) 17–21, https://doi.org/10.1016/j.commatsci.2012.04.026.
[18] X. Yang, S. Marie, C. Jacquemoud, P. Bompard, Prediction of cleavage crack propagation path in a nuclear pressure vessel steel, Eng. Fract. Mech. 191 (December) (2018) 486–503.
[19] C. Berdin, 3D modeling of cleavage crack arrest with a stress criterion, Eng. Fract. Mech. 90 (2012) 161–171, https://doi.org/10.1016/j.engfracmech.2012.05.002.
[20] A. Dahl, C. Berdin, D. Moinereau, Dynamic modeling of cleavage crack propagation and arrest with a local approach, Proc. Eng. 10 (2011) 1853–1858, https://doi.org/10.1016/j.proeng.2011.04.308.
[21] R.O. Ritchie, J.F. Knott, J.R. Rice, On the relationship between critical tensile stress and fracture toughness in mild steel, J. Mech. Phys. Solids 21 (6) (1973) 395–410, https://doi.org/10.1016/0022-5096(73)90008-2.
[22] S. Aihara, Y. Tanaka, A simulation model for cleavage crack propagation in bcc polycrystalline solids, Acta Mater. 59 (11) (2011) 4641–4652.
[23] K. Shibanuma, Y. Suzuki, K. Kiriyama, K. Suzuki, H. Shirahata, A model of cleavage crack propagation in a BCC polycrystalline solid based on the extended finite element method, Acta Mater. 176 (2019) 232–241.
[24] Y. Qiao, A.S. Argon, Cleavage cracking resistance of high angle grain boundaries in Fe-3%Si alloy, Mech. Mater. 35 (3–6) (2003) 313–331.
[25] Y. Qiao, A.S. Argon, Cleavage crack-growth-resistance of grain boundaries in polycrystalline Fe-2%Si alloy: experiments and modeling, Mech. Mater. 35 (1–2) (2003) 129–154.
[26] T. Handa, T. Tagawa, F. Minami, Correlation between charpy transition temperature and brittle crack arrest temperature considering texture, Tetsu-To-Hagane/J. Iron Steel Inst. Japan 98 (1) (2012) 32–38, https://doi.org/10.2355/tetsutohagane.98.32.
[27] T. Handa, S. Igi, K. Oi, et al., Effect of toughness distribution in the thickness direction on long brittle crack propagation/arrest behaviour of heavy gauge shipbuilding steel, Weld Int. 32 (7) (2018) 460–468, https://doi.org/10.1080/01431161.2017.1346884.
[28] J. Taylor, P. Moore, A. Mehmanparast, R. Kulka, Correlation between steel microstructural characteristics and the initiation and arrest toughness determined from small-scale mechanical testing, in: Proc Int Conf Offshore Mech Arct Eng – OMAE, vol. 4(November), 2019, https://doi.org/10.1115/OMAE2019-95290.
[29] J. Taylor, A. Mehmanparast, R. Kulka, P. Moore, Correlation between steel initiation toughness and arrest toughness determined from small-scale mechanical testing, Procedia Struct. Integr. 17 (September) (2019) 472–478, https://doi.org/10.1016/j.prostr.2019.08.062.
[30] T. Kobayashi, Dynamic photoelastic determination of the a(dot)-K relation for 4340 alloy steel, in: G.T. Hahn, M.F. Kanninen (Eds.), Crack Arrest Methodology and Applications, ASTM STP 711, American Society for Testing and Materials, 1980, pp. 189–210.
[31] J. Kalthoff, Experimental analysis of dynamic effects in different crack arrest test specimens, in: G.T. Hahn, M.F. Kanninen (Eds.), Crack Arrest Methodology and Applications, ASTM STP 711, American Society for Testing and Materials, 1980, pp. 109–127.
[32] J.A. Joyce, R.E. Link, C. Roe, J.C. Sobotka, Dynamic and static characterization of compact crack arrest tests of navy and nuclear steels, Eng. Fract. Mech. 77 (2) (2010) 337–347, https://doi.org/10.1016/j.engfracmech.2009.04.006.
[33] ASTM, E1221 Standard Test Method for Determining Plane-Strain Crack-Arrest Fracture Toughness, K Ia, of Ferritic Steels. 96(Reapproved) (2007) 1–19. https://doi.org/10.1520/E1221-12A.2.
[34] ASTM, E208 Standard Test Method for Conducting Drop-Weight Test to Determine Nil-Ductility Transition Temperature of Ferritic Steels 1. Test, 2000;06(Reapproved):1-13. https://doi.org/10.1520/E0208-06R12.2.
[35] Pb C, Ej R. Comparison of Crack Arrest Methodologies, Published online 1980, pp. 211–227.
[36] EDF Energy UK, R6. Assessment of the Integrity of Structures Containing Defects, 2006.
[37] G. Green, J.F. Knott, On effects of thickness on ductile crack growth in mild steel, J Mech Phys Solids 23 (3) (1975), https://doi.org/10.1016/0022-5096(75)90014-9.
[38] T. Handa, S. Igi, K. Oi, K. Nishimura, H. Tajika, T. Tagawa, Effect of Toughness Distribution in the Thickness Direction on Long Brittle Crack Propagation/Arrest Behavior of Heavy Gauge Shipbuilding Steel Brittle Crack Arrestability of Test Steels Arrestability of Test Steels under Condition of No, Published online 2016, pp. 126–131.
[39] K. Sugimoto, Thickness effect on brittle crack arrest toughness value (Kca)-6, in: ISOPE - 20th International Offshore and Polar Engineering Conference, 2010.
[40] K. Wallin, The size effect in KIC results, Eng. Fract. Mech. 22 (1) (1985) 149–163, https://doi.org/10.1016/0013-7944(85)90167-5.
[41] R. Marschall, Specimen-Size Considerations in Crack-Arrest Testing of Irradiated RPV Steels, Published online 1986, pp. 339–352.
[42] Society JWE, JWES 2815:2014 Test Method for Brittle Crack Arrest Toughness Kca, 2014.
[43] E1921-15ae1, Standard Test Method for Determination of Reference Temperature, To, for Ferritic Steels in the Transition Range, in: ASTM Book of Standards, 2016, pp. 1–23. https://doi.org/10.1520/E1921-15AE01.2.
[44] X.K. Zhu, J.A. Joyce, Review of fracture toughness (G, K, J, CTOD, CTOA) testing and standardization, Eng. Fract. Mech. 85 (2012) 1–46, https://doi.org/10.1016/j.engfracmech.2012.02.001.
[45] Y. Funatsu, H. Shirahata, J. Otani, T. Inoue, Y. Hashiba, The effect of shear-lips on the arrestability of thicker steel plates longitudinal, Isope 4 (2012) 63–66.
[46] P.B. Crosley, WELDING RESEARCH Crack Arrest Fracture Toughness of a Structural Steel (A36), Published online 1982.
[47] C.S. Wiesner, Predicting structural crack arrest behaviour using small scale material characterisation tests, Int. J. Pres. Ves. Pip., Published online 1995.
[48] A. Willoughby, Crack arrest concept, in: Proc Semin Eng Performance Welded Joints, Published online 1986.
[49] G. Hahn, Crack Arrest Methodology and Applications, Am. Soc. Test Mater., Published online 1980.
[50] W. Pellini, P. Puzak, Fracture analysis diagram procedures for the fracture-safe engineering design of steel structures, Weld Res. Counc. Bull. 88 (1963).
[51] T. Robertson, Propagation of brittle fracture in steel, J. Iron Steel Inst. 175 (1953).
[52] Institution BS. BS18:1987: Method for Tensile Testing of Metals, 1987.
[53] Institution BS, BS EN10045:1990: Charpy Impact Test on Metallic Materials, 1990.
[54] Materials AS for T and. ASTM E436-86: Standard Method for Drop Weight Tear Tests of Ferritic Steels, 1986.
[55] C.S. Wiesner, B. Hayes, A.A. Willoughby, Crack Arrest in Modern Steels and their Weldments Comparison between Small and Large Scale Experiments 56 (1993) 369–385.
[56] K. Avenue, S. Kt, C. Berkeley, N. Laboratories, G. Gli, R6. Assessment of the integrity of structures containing defects, Construction 32 (1988) 3–104.
[57] P. Puzak, E. Eschbacher, W. Pellini, Initiation and propagation of brittle fracture in structural steels, Weld J. 31 (12) (1952) 561–581.
[58] M.T. Kirk, M.E. Natishan, M. Wagenhofer, et al., A Summary of Wallin's Empirical Findings. Published online, 2002, pp. 729–740.
[59] R.E. Link, J.A. Joyce, C. Roe, Crack arrest testing of high strength structural steels for naval applications q, Eng Fract Mech 76 (3) (2009) 402–418, https://doi.org/10.1016/j.engfracmech.2008.11.006.
[60] K.K. Toon, Fracture toughness data analysis using the master curve method, WRC Bull 486 Part 3, Nov 2003, Published online, 2003.
[61] C.E. Pugh, W.R. Corwin, S. Rhbryanbrbas. C.e. pugh, w.r. corwin, r.h. 96 (1986) 297–312.
[62] K. Wallin, P. Karjalainen-roikonen, Crack arrest toughness estimation for high strength steels from sub-sized instrumented Charpy-V tests, in: Proc Twenty-sixth Int Ocean Polar Eng Conf. Published online, 2016, pp. 85–91.
[63] ISO, ISO 148-1:2006: Metallic materials – Charpy pendulum impact test – Part 1: Test method. ISO. Published online, 2006.

[64] ISO, BS EN ISO 6892-1:2016 BSI Tensile Testing Part 1 : Method of Test at Room Temperature, 2016.
[65] BSI, BS EN 10164:2004 Steel Products with Improved Deformation Properties Perpendicular to the Surface of the Product — Technical Delivery Conditions, 2004.
[66] Y. Yamamoto, Multiscale modeling to clarify the relationship between microstructures of steel and macroscopic brittle crack microstructures of steel and macroscopic brittle crack propagation/arrest behavior modeling of a high, Proc. Struct. Integr. 2 (2016) 2389–2396, https://doi.org/10.1016/j.prostr.2016.06.299.
[67] JFE Steel. Product: Crack Arrest Steel Plate. https://www.jfe-steel.co.jp. Published 2020 [accessed April 15, 2020] https://www.jfe-steel.co.jp/en/products/plate/b02.html.
[68] ASTM, E112-19 Standard Test Methods for Determining Average Grain Size, 2019. https://doi.org/10.1520/E0112-13.1.4.
[69] ISO, BS7448-1: Fracture mechanics toughness tests, BS EN, 1991 (November).
[70] A. Mehmanparast, J. Taylor, F. Brennan, Experimental investigation of mechanical and fracture properties of offshore wind monopile weldments: SLIC interlaboratory test results, Fatigue Fract. Eng. Mater. Struct. (April) (2018) 1–17, https://doi.org/10.1111/ffe.12850.
[71] C.D. Ingelbrecht, M. Loveday, The Certification of Ambient Temperature Tensile Properties of a Reference Material for Tensile Testing According to EN 10002-1, CRM661, 2000.
[72] J.D. Lord, B. Roebuck, L. Orkney, Validation of a Draft Tensile Testing Standard for Discontinuously Reinforced MMC, VAMAS Report No.20, 1995.
[73] British Standards Institution. EN 1011-2. Welding - Recommendations for Welding of Metallic Materials - Part 2: Arc Welding of Ferritic Steels, 2001.
[74] C. Wang, M. Wang, J. Shi, W. Hui, H. Dong, Effect of microstructural refinement on the toughness of low carbon martensitic steel, Scr. Mater. (2008), https://doi.org/10.1016/j.scriptamat.2007.10.053.
[75] J.M. Hyzak, I.M. Bernstein, The role of microstructure on the strength and toughness of fully pearlitic steels, Metall. Trans. A (1976), https://doi.org/10.1007/BF02656606.
[76] D.A. Curry, J.F. Knott, The relationship between fracture toughness and microstructure in the cleavage fracture of mild steel, Met. Sci. (1976), https://doi.org/10.1179/030634576790431453.